THE ASTROPHYSICAL JOURNAL, 241:507–520, 1980 October 15

THE DOUBLE QUASAR Q0957+561 A, B: A GRAVITATIONAL LENS IMAGE FORMED BY A GALAXY AT $z=0.39$

PETER YOUNG,[1] JAMES E. GUNN,[1] JEROME KRISTIAN,[2] J. B. OKE,[1] AND JAMES A. WESTPHAL[1]
Received 1980 January 28; accepted 1980 April 3

ABSTRACT

We believe that we have observed the gravitational lens that is responsible for producing the double quasar. Extremely deep CCD pictures of the region show that the QSOs are behind a rich cluster of galaxies. The CCD data and spectrophotometry of the QSOs indicate that the southern QSO image is seen through the brightest cluster galaxy, whose redshift is 0.39.

Calculations of gravitational imaging by King model mass distributions show that the cluster and the brightest galaxy together, acting as a gravitational lens on the light from a single, more distant QSO, can easily reproduce all of the present observations.

We conclude that the double quasar is almost certainly the multiple image of a single object produced by a gravitational lens.

Subject headings: galaxies: clusters of — galaxies: general — gravitation — quasars

I. INTRODUCTION

The pair of QSOs Q0957+561 A, B were identified by Walsh, Carswell, and Weymann (1979), and additional spectroscopic observations were reported by Weymann *et al.* (1979); these authors suggested that the object is a single QSO at $z=1.41$ with a double image produced by an intervening galaxy acting as a gravitational lens.

In order to search for the galaxy, we took a series of deep red pictures of the QSO field in good seeing with a CCD camera on the 200 inch (5 m) telescope. These show a rich cluster of galaxies, whose brightest member is nearly superposed on Q0957+561 B. Multichannel scans of the QSO show a contribution from this galaxy, and the location of the characteristic 4000 Å break in the galaxy spectrum gives a redshift of 0.39.

We have calculated in some detail the gravitational imaging of the QSO expected from the galaxy and the cluster. The galaxy alone, approximated by a plausible King (1966) model and with a reasonable velocity dispersion, would be expected to produce a situation very much like that observed. There is a clear prediction in this simple case that the QSO component (B) nearest the galaxy should itself be double, with a separation of order 0.″2 and with comparable brightness for the subcomponents. The effect of the cluster, whose parameters are quite uncertain, is to complicate the picture severely; the cluster effects cannot be neglected for any plausible set of parameters. The central region of the cluster is, however, a positive lens and helps the galaxy create multiple images. With the introduction of the cluster, there are a number of different configurations which produce images like the observed ones, and sorting out which situation prevails will require further, very difficult, observations.

What does emerge clearly is that the galaxy-cluster combination should make multiple images, and that there are several plausible ways to reproduce the observations. We regard the case for the correctness of some one of these to be very good.

[1]Palomar Observatory, California Institute of Technology.
[2]Mount Wilson and Las Campanas Observatories, Carnegie Institution of Washington.

II. OBSERVATIONS

a) Instrumentation

The photometry described here was obtained with PFUEI, an image-reducing CCD camera/spectrograph described by Gunn, Hoessel, and Westphal (1980). The PFUEI reimages the f/3.52 prime focus image of the 200 inch Hale telescope (equipped with the five-element Wynne field corrector) onto the CCD at f/1.4, providing a match of the seeing disk to the 15 μm pixels of the CCD. The resulting scale is 0.″42 per pixel. The CCD is an experimental Texas Instruments chip, which has an array of 500×500 picture elements in a thinned, back-illuminated, buried channel configuration. The readout noise is about 15 electrons (rms), and dark current is reduced to negligible levels by cooling to $-120°$ C with liquid nitrogen. All the transmission optics are low-reflection coated except the dewar window, and the detective quantum efficiency of the system including the telescope is 40% in the red.

The spectrophotometry from which we obtained the galaxy redshift was done with the multichannel spectrophotometer described by Oke (1969).

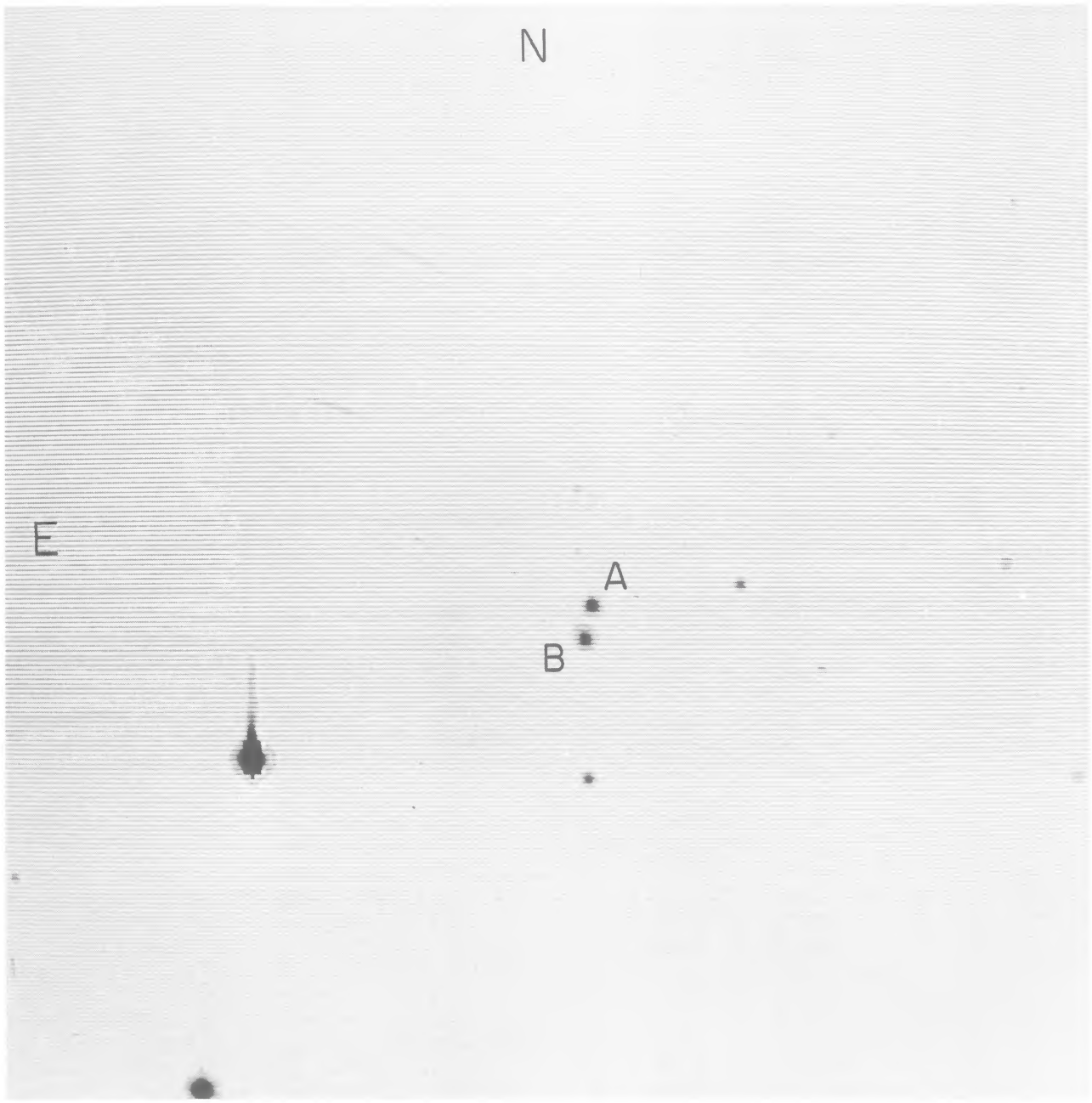

FIG. 1*a*

FIG. 1. (*a*, *b*).—CCD data on the double QSO Q0957+561 A, B and the surrounding cluster. We present two pictures of the same frame with different gray scales to show (*a*) the double QSO images, (*b*) the galaxies in the cluster. 86% of the objects on the frame are galaxies as determined using Sebok's (1979) algorithm. A marked concentration of galaxies surrounds the QSOs and extends W to the edge of the frame. Another concentration extends to the NE. The frame is 200″ square; N is up and E is left. The limiting magnitude is $m_r \sim 26$. Components A and B of the double QSO are marked in Fig. 1*a*. Galaxies G1–G5 in the surrounding cluster are marked in Fig. 1*b*.

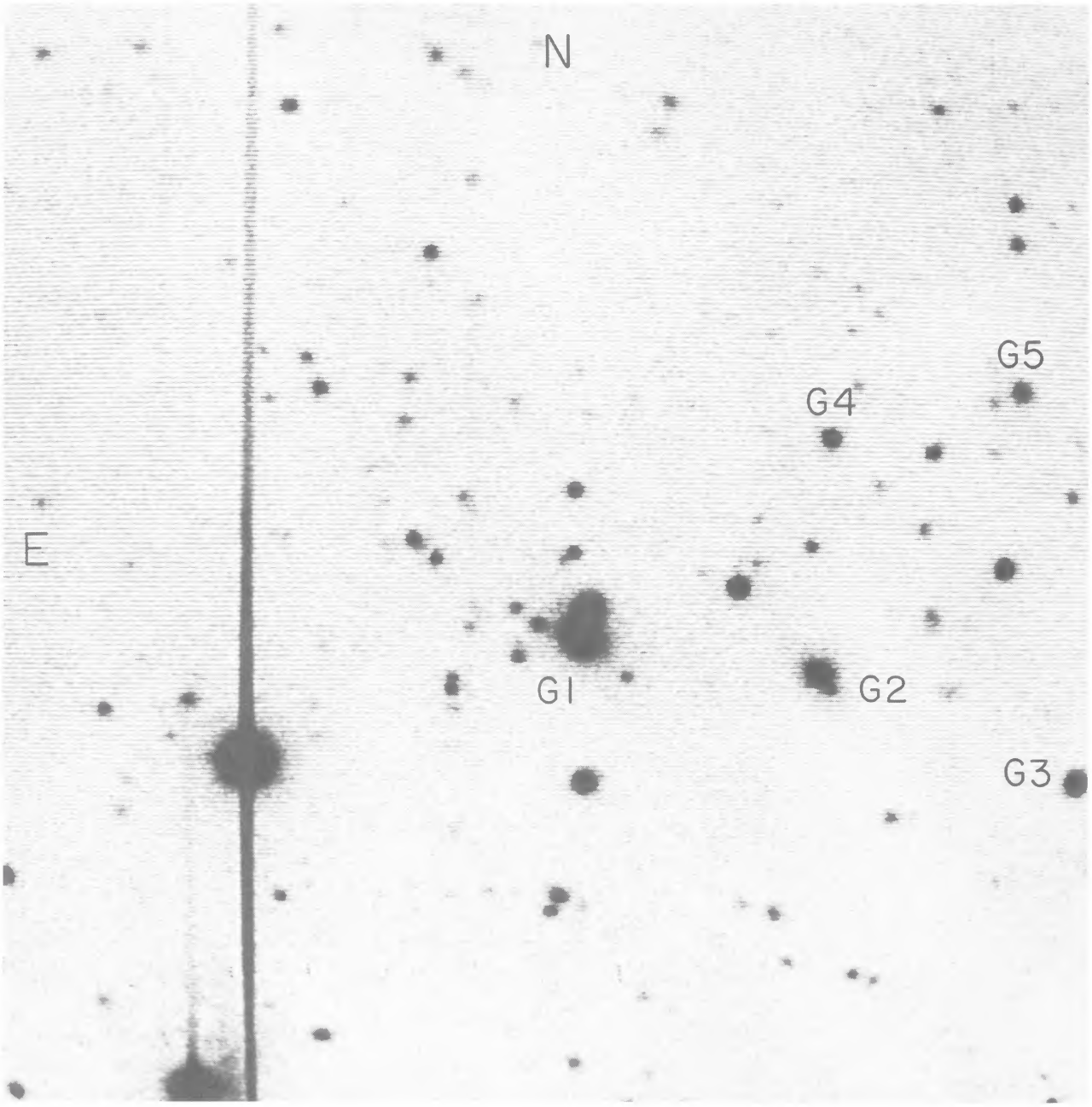

FIG. 1*b*

b) *CCD Observations and Reductions*

The field of Q0957+561 A, B was observed in a 2 hour period starting at 1979 November 15.469. Twenty-two exposures of 300 s each were taken. The filter was 3 mm of Schott RG610 with a short-pass interference coating, giving a roughly rectangular bandpass from 6100 to 7000 Å. The response approximates that of *r* in the *uvgr* system (Thuan and Gunn 1976). The data are shown in Figure 1 at two contrast levels to emphasize separately the QSOs (*a*), and the galaxy and cluster (*b*).

The CCD reduction procedure was essentially as described in Young *et al.* (1979).

Photometric calibration was done using standard stars of the *uvgr* system, with improved magnitudes measured by Kent (1979, private communication). Five standards with a large spread in color yielded the relation

$$r_T = r + 0.110(g_T - r_T) + C, \quad (1)$$

where r = natural CCD magnitude, r_T, g_T = standard star magnitudes in the *uvgr* system. Equation (1) is consistent with the CCD response in the red being enhanced relative to the S20 photocathode with which the photometric system was defined. Examination of the series of exposures on Q0957+561 A, B showed a scatter due to the presence of thin cirrus of 3%, which we adopt as our estimate of the photometric accuracy.

c) *Radial Profiles of Q0957+561 A, B*

Upon examining the stacked data frames, the southern QSO (Q0957+561 B) was seen to be extended at low surface brightness levels when compared with the northern QSO and field stars on the same frame. Excess light is smoothly distributed and slightly offset toward the other QSO image.

Image profiles were obtained and are shown in Figure 2. Stars on the frame were used to define a seeing profile. The seeing was good (FWHM = 0.″98), and the star images were reasonably circular.

The northern QSO (Q0957+561 A) has a stellar profile except for a very slight luminosity excess at $r > 4''$, which may well be due to uncertainty in the determination of the sky level. The southern QSO (Q0957+561 B) is obviously extended relative to the other QSO and to the star shown in Figure 2.

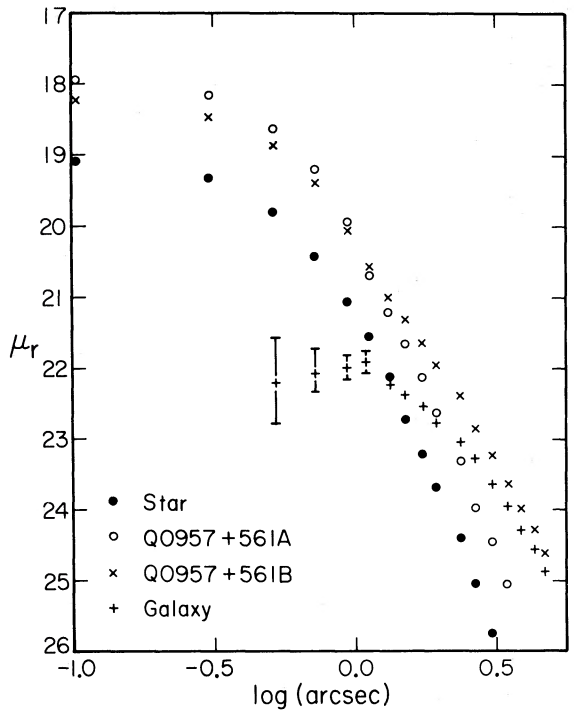

FIG. 2.—Azimuthally averaged luminosity profiles of Q0957+561 A and B, and of the galaxy surrounding the image of Q0957+561 B (obtained by subtracting 0.76 times A from B). Also shown is a star to define the seeing profile. In the seeing with FWHM of 1″, Q0957+561 A is a point source. μ_r is magnitudes per arcsec^2 at λ6550.

Figure 3 shows contour levels for the data around the two QSO images. It may be seen that the image of A is circular at low brightness levels, but the outer contours of B are extended, elliptical, and displaced toward component A. The ellipticity is 0.13 with the major axis roughly 60° to the line joining the QSOs.

The core of image B is 0.76 times as bright as A. When image A is multiplied by 0.76 and subtracted from B, the resulting profile is flat within a radius of 1.″6 and then drops slowly. This is also plotted in Figure 2. We shall call this image "the galaxy" or "G1" in what follows: We will argue that it is the brightest galaxy of the cluster.

The centers and magnitudes for the three images, in a rectangular coordinate system in which y increases northward and x westward, are

Q0957+561 A: $x = +1.''21 \pm 0.''01$,
$y = +6.''03 \pm 0.''01$,
$m_R = 17.33 \pm 0.03$.

Q0957+561 B: $x = 0.''00$,
$y = 0.''00$,
$m_r = 17.62 \pm 0.03$.

Galaxy: $x = +0.''02 \pm 0.''06$,
$y = +0.''78 \pm 0.''12$,
$m_r \sim 18.5$.

The galaxy was measured at the $\mu_r = 23.0$ contour level where interference from the two QSOs is minimal. The galaxy ellipticity is 0.13 ± 0.01, and the position angle of its major axis is $53° \pm 5°$. The QSO magnitudes were measured using the center of the profile only; the galaxy is not included in the magnitude for Q0957+561 B. The ratio of brightness of the QSO images is accurate to about 2%.

Note that the galaxy is slightly, but significantly, offset from the exact line joining the QSOs. Our position for the galaxy had to be measured at a low brightness level to get away from the effects of Q0957+561 B. If the isophotes are distorted, we may not be measuring the position of the galaxy center.

The extended image was also observed by Adams and Boroson (1979), who suggested that it was physically associated with Q0957+561 B. The "excess flux" between the QSOs seen by these authors can be explained by the displacement of the galaxy image to the north of B. We can rule out the existence of another object between the QSOs at a level $m_r \sim 25$.

Alan Stockton (1979, private communication) has recently sent us copies of direct plates taken by him in

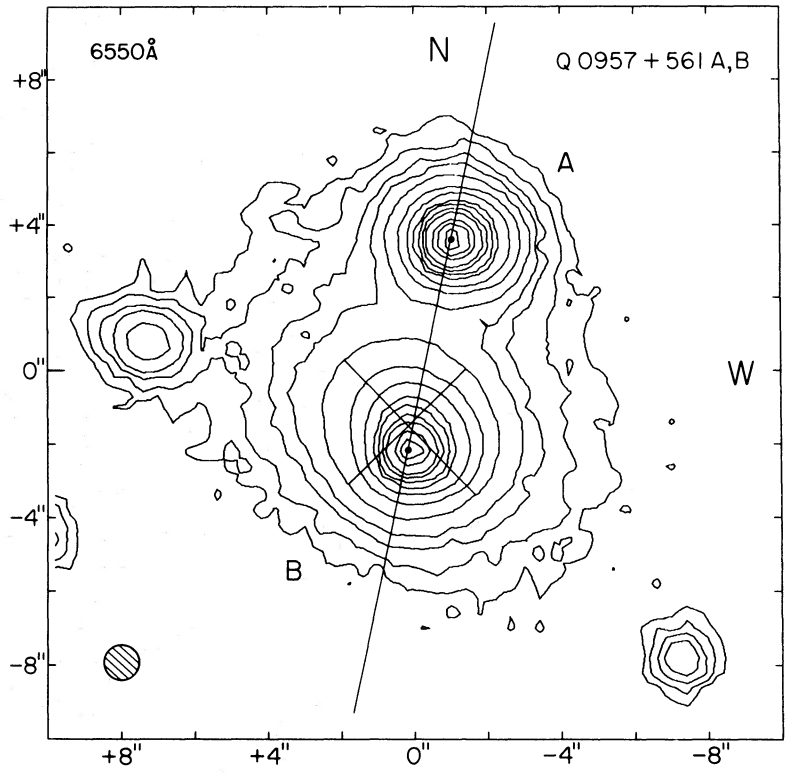

FIG. 3.—Contour map of Q0957+561 A, B from the CCD data. The contour intervals are not quite uniform, but are (roughly) 0.5 mag. The illustrated beam size is 0.″98. Q0957+561 A is unresolved, whereas Q0857+561 B (which is fainter by 0.29 mag) is extended at faint levels. The "x" shaped pair of lines near B are the major and minor axes of the brightest galaxy of the surrounding cluster. The galaxy centroid is 0.″78 north of Q0957+561 B and is slightly offset from the line joining the QSOs, whose centers are indicated by black dots. Other galaxies in the surrounding cluster are visible to the E and SW.

extremely good seeing at Mauna Kea. These plates resolve B and the nucleus of the galaxy.

d) Cluster of Galaxies Surrounding Q0957+561 A, B

There is a large, rich cluster of galaxies surrounding the twin QSOs which is shown well in Figure 1*b*. The extended image underlying Q0957+561 B looks very much like the brightest cluster member. The next brightest galaxy on our frame (G2) is located 5.″0 S and 42.″0 W of Q0957+561 B. Both G1 and G2 exhibit the extended, low surface brightness halos typical of the brightest galaxies in clusters. This can be seen in Figure 4, where we have plotted the aximuthally averaged profiles of G1 through G5.

We shall in § III*b* derive a core radius of 3 kpc for the galaxy on the gravitational lens hypothesis. A King model for a galaxy with this core radius and $\varepsilon_T = 9$ was constructed and fitted to the profile (see Fig. 4). This model also fits the Coma cluster galaxies N4874 and N4889 (see Young *et al.* 1979). Note that the model was convolved with the seeing disk and then offset by 0.″75 before taking the profile, because the galaxy center is displaced from Q0957+561 B where the profile is centered.

The position of the cluster center is of crucial interest, as we shall see later. To obtain this, we counted galaxies on the frame with $m_r \lesssim 23$ and plotted the distribution in x and y separately (the cluster is elongated and aligned roughly EW). The deduced cluster center is 15″ ± 7″ N and 2″ ± 20″ W of Q0957+561 B, and the core semimajor axes are 26″ (NS) by 51″ (EW). This gives it dimensions 150 kpc by 300 kpc since 1 kpc = 0.″171 at $z = 0.39$ with $q_0 = 0$ and $H_0 = 60$ km s^{-1} Mpc^{-1}.

Adams and Boroson (1979) observed eight of the galaxies immediately around the twin QSOs, but concluded that it was unlikely that a rich cluster was present. The cluster we have observed would not, perhaps, be as striking with their smaller field and brighter limiting magnitude.

e) Spectrophotometry

Data were obtained on 1979 May 1.21 UT with the Multichannel Spectrophotometer (MCSP) on the Hale telescope. A 7″ diameter aperture was used to measure each of the components of the double quasar, with

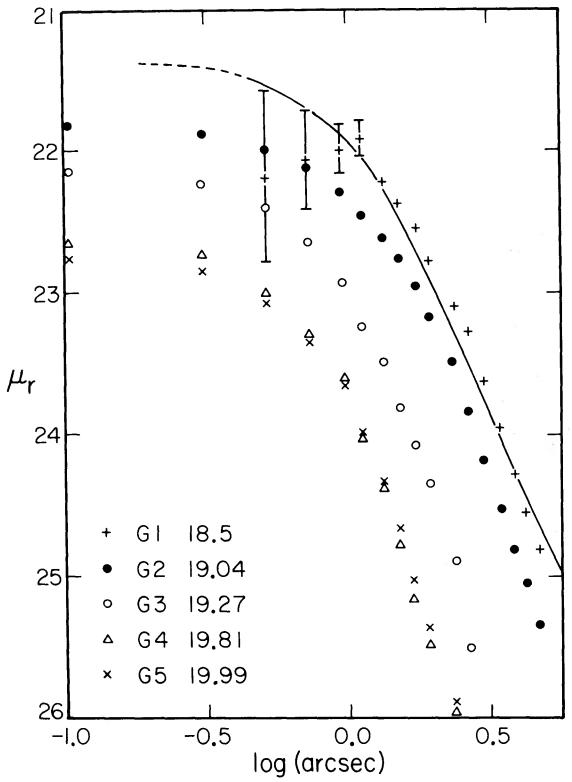

FIG. 4.—Aximuthally averaged profiles of the five brightest galaxies in the cluster surrounding Q0957+561 A, B. The brightest galaxy (G1) is the one superposed on Q0957+561 B, and G2 is 5″ S and 41″ W of Q0957+561 B. Both G1 and G2 show the characteristic extended halos of the brightest galaxies in clusters. Galaxies G3, G4, and G5 (whose profiles are offset down 1 mag to reduce confusion) lack such halos. This can be seen by comparing the vertical displacements between the curve as a function of radius. The quantity μ_r is magnitude per arcsec^2 at λ6550 (or λ4700 in the galaxy rest frame). Galaxy G1 has been fitted with a King model (the same model also fits N4874 and N4889 in the Coma cluster). The details of the core of G1 are very sensitive to the adjusted brightness ratio of A to B.

total integration times of 1000 s on each object. The seeing was 1″. The resolution was 40 Å in the blue and 80 Å in the red.

The measurements of Q0957+561 B include essentially all the light from the galaxy ($m_r \sim 18.5$) within the 7″ aperture. The aperture used for Q0957+561 A probably includes a very small contribution from the galaxy. The fluxes are plotted against λ in Figure 5. Emission lines of Mg II λ2799, C III] λ1909, and C IV λ1549 at a redshift of $z=1.41$ are seen in both spectra and are of comparable equivalent width (see below). In component B there is a sharp break in the continuum level of the spectrum somewhere between 5500 and 5750 Å, which we interpret as being caused by the H and K Ca II break in the spectrum of the superposed galaxy. The fitting of the galaxy spectrum, described below, is consistent with the break being at 5500 Å, corresponding to $z=0.39$. The spectrum by Walsh, Carswell, and Weymann (1979) is consistent with this redshift. The break is scarcely visible in the data of Wills and Wills (1980), who used a small (2″×3″) aperture. This supports our contention that the break is in the light from the galaxy and is not in the quasar light.

Assuming that quasars A and B are identical, and that A represents the spectra of both quasars, it is possible to decompose the spectrum of B into galaxy and quasar. This produces a net galaxy spectrum which agrees well with normal giant elliptical galaxies provided that quasar B has an intensity of 0.72 ± 0.02 of that of A, compared with the ratio of 0.76 ± 0.02 found above from analysis of the direct pictures. The galaxy fit yields a redshift of 0.39 with an estimated error of about 0.02. The best fit of the multichannel data for component B gives 5, 14, 28, and 32% of the radiation attributable to the superposed galaxy at 4140, 5080, 6120, and 7520 Å, respectively.

The emission line equivalent widths of C IV λ1550, C III] λ1909, and Mg II λ2800 are 77, 62, and 58 Å, respectively, for component A, and 74, 58, and 45 Å for component B. When the equivalent widths in B are referenced to quasar B continuum only, the equivalent widths become 74, 64, and 64 Å, respectively, in excellent agreement with those for component A.

The brightness and size of the galaxy cluster are fully consistent with a redshift of 0.39. Further, the brightest galaxy G1 has, in the standard aperture of Hoessel, Gunn, and Thuan (1980), a magnitude $m_r=18.93$. Translating to their magnitude system places the galaxy in the band defined by brightest cluster galaxies in the Hubble diagram.

The magnitude difference between the two QSOs from the MCSP data is 0.34 mag at λ3700 where the galaxy contribution is negligible ($AB_{3700}=17.62$ and 17.96 for Q0957+561 A and B, respectively). The CCD photometry indicated a difference of 0.30 mag; no real case can be made for variability. Further, after removing a galaxy component from the MCSP data there is no evidence for reddening of one QSO as compared with the other.

III. GRAVITATIONAL BENDING OF LIGHT RAYS PASSING THROUGH EXTENDED MASS DISTRIBUTIONS: MODELS FOR THE LENS

We believe that Walsh, Carswell, and Weymann (1979) were correct, when they suggested that the double quasar is a double image of a single object formed by a gravitational lens. Discussions of this object have assumed that the near equality of the brightnesses of the two images necessarily implied that the lens must lie nearly midway between them. Most of the classical work on gravitational lenses has been done with point-

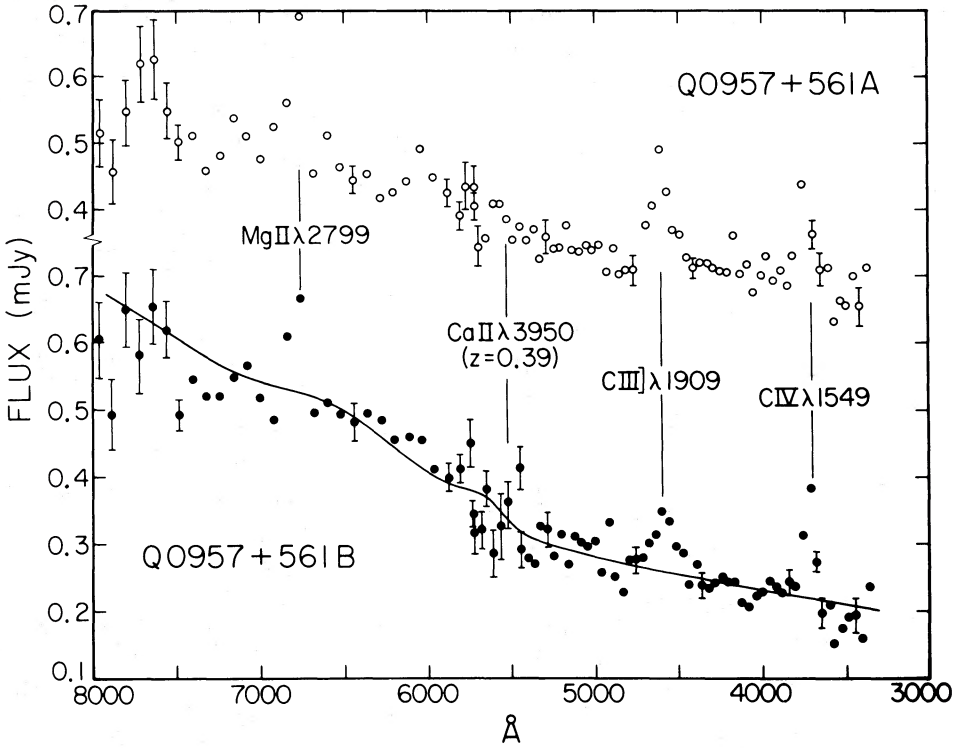

FIG. 5.—Multichannel spectrophotometry of Q0957+561 A, B. Each object was observed for 1000 s with a 7″ aperture. The QSO emission lines of Mg II λ2799, C III] λ1909, and C IV λ1549 at $z=1.41$ are clearly visible. The break in the spectrum of Q0957+561 B at λ5500 due to the galaxy light is very pronounced, and gives a redshift for the galaxy of 0.39. The line drawn through the spectrum of Q0957+561 B is the sum of 0.72 times Q0957+561 A plus a standard brightest cluster galaxy. A flux of 0.1 mJy corresponds to $AB_\nu = 18.91$.

mass lenses, for which this conclusion is correct. It is not true, however, for lenses consisting of extended mass distributions *through which* the light passes. We shall see that the observed situation is easily reproduced with a lens galaxy situated, as G1 is, in close proximity to one of the images. We begin this section with a qualitative overview of the lens model, and then discuss detailed models for the imaging due to the galaxy and for the galaxy and cluster combined.

a) Transparent Lenses: A Qualitative Overview

The general theory of spheroidal transparent lenses has been developed by Bourassa and Kantowski (1975). The treatment here is much simpler but will deal with mass distributions representative of real galaxies. In the limit in which light is deflected by passage through or around a galaxy in which the velocities are small compared to the velocity of light, the bending angle is small (of order v^2/c^2) and can be evaluated by integration of the gravitational acceleration perpendicular to the unperturbed light path. The vector bending angle is

$$\boldsymbol{\alpha} = 2c^{-2}\int \nabla\Phi \, dl, \tag{2}$$

where Φ is the Newtonian potential; $\boldsymbol{\alpha}$ is well defined if the distance through the lens is small compared to the total light path.

We will assume spherically symmetric mass distributions for both the galaxy and the cluster; for the galaxy because the effects of its ellipticity have been investigated and found to be negligible, and for the cluster because the data do not warrant better treatment. For a spherically symmetric mass, the scalar bending angle is

$$\alpha = 4c^{-2}b\int_b^\infty dr \frac{d\Phi}{dr}(r^2-b^2)^{-1/2} \tag{3a}$$

$$= 4G\mathfrak{M}(b)b^{-1}c^{-2}, \tag{3b}$$

where b is the impact parameter, and $\mathfrak{M}(b)$ is the projected mass interior to b.

For physically reasonable, nonsingular mass distributions, α does not diverge at $b=0$, as it does for a point mass. Instead, $\alpha \to 0$ as b approaches 0 or $\pm\infty$. For galaxy models, the falloff at large impact parameter is slow.

Figure 6*a* shows a schematic diagram in Euclidean space (we discuss relativistic cosmology later in this

section) of the geometry of the bending process. For a beam which passes on the other side of the lens, the equations derived below will still hold if the angles θ and α are taken to be negative. If the angles are small, we must have

$$D_s\theta_Q + D_{ds}\alpha = D_s\theta. \tag{4}$$

But

$$\alpha = \alpha(b) = \alpha(D_d\theta) \tag{5}$$

is defined by equation (3) for a given mass distribution. Images will then be found at angles which are solutions of

$$\alpha(D_d\theta) = (D_s/D_{ds})(\theta - \theta_Q). \tag{6}$$

This is illustrated schematically in Figure 6*b*, in which a physically reasonable form for $\alpha(b)$ is drawn along with the straight line given by the right-hand side of equation (6). Solutions (images) correspond to intersections of the curve and the line. It is clear that for any function $\alpha(b)$ which is continuous and for which $|d\alpha/db| \to 0$ as $b \to \pm\infty$, there must be an odd number of solutions. For functions like that shown, there must be either one image (if θ_Q is large enough or the lens is too weak to bend *any* ray with negative b back to the observer) or three images, except in the special singular case of the straight line being just tangent to $\alpha(D_d\theta)$. That the image multiplicity must be odd can be proved for general bounded transparent lenses; it does not require spherical symmetry.

Since the specific intensity along any ray is conserved, the brightness of any image is proportional to the ratio of the solid angle in the image plane to the corresponding solid angle in the object plane. If $\boldsymbol{\theta}$ is a vector angle in the image plane and $\boldsymbol{\theta}_Q$ the corresponding angle in the object plane, then

$$I/I_0 = \left[J(\boldsymbol{\theta}_Q, \boldsymbol{\theta}) \right]^{-1}, \tag{7}$$

where I is the observed brightness (flux), I_0 is the brightness which would have been observed with no lens, and $J = \partial(\boldsymbol{\theta}_Q)/\partial(\boldsymbol{\theta})$ is the Jacobian of the transformation from $\boldsymbol{\theta}$ to $\boldsymbol{\theta}_Q$. In the spherically symmetric case, this becomes

$$I/I_0 = (\theta/\theta_Q)(d\theta/d\theta_Q) \tag{8}$$

$$= \frac{\theta}{\theta_Q} \frac{D_s/D_{ds}}{D_s/D_{ds} - D_d\, d\alpha(b)/db}. \tag{9}$$

If I/I_0 is negative, the images are mirror-reversed. The brightness of an image is proportional to its angular distance θ from the lens and inversely proportional to

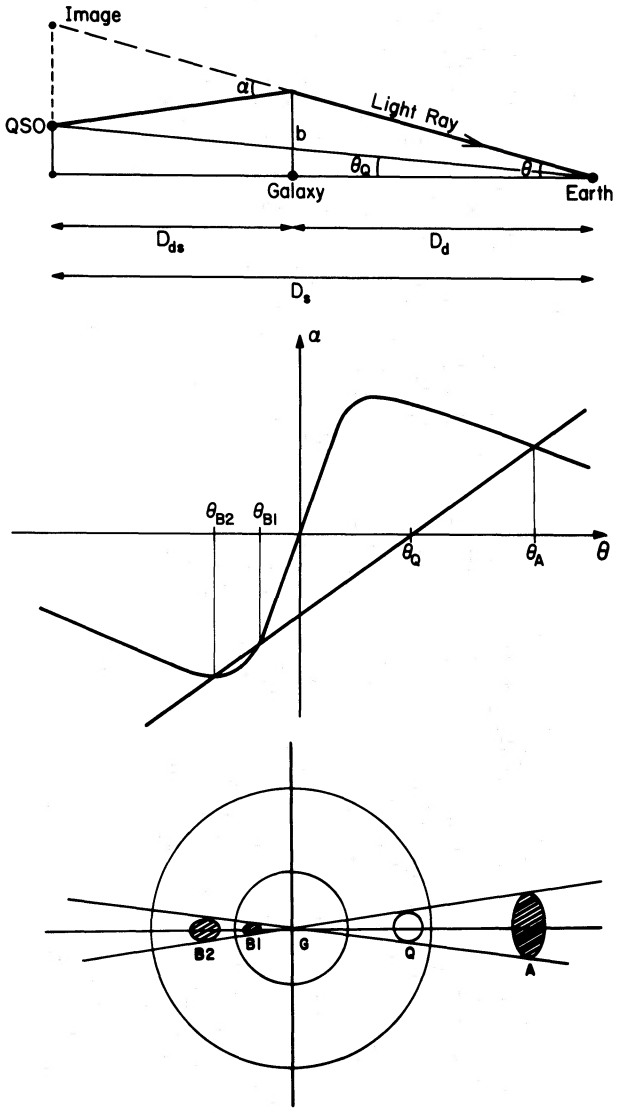

FIG. 6.—Schematic diagram of lens models. In the upper part of the diagram we show the nomenclature for distances and angles. In the middle part we show the bending angle α as a function of image displacement θ (or equivalently the impact parameter b). Image solutions θ for given θ_Q are determined by the intercept of straight line and α-curve as discussed in the text. Note that there must be one or three image solutions for any θ_Q (there can never be only two solutions). We have drawn the case in which image B is a close double near the galaxy, while A is well removed from the galaxy. The true QSO position then lies roughly halfway between the galaxy and image A. In the lower part of the figure we show the true position of the QSO (circle Q) and its three images. Note that image A is extended perpendicular to the galaxy–QSO line and that images B1, B2 are extended along it. The surface area of B1 and B2 can quite easily equal that of A, giving equal brightness for Q0957+561 A, B despite their very different separations from the galaxy G. Two large circles are also shown. The outer one is the "singular circle." The true QSO position must lie within this circle to form three images; if it lies outside, there will be only one image. The inner circle is where the two extra images will appear if Q lies on the singular radius. As Q moves inside the singular radius, the extra two images move away from, and straddle, the inner circle.

the difference of the derivative of the curve $\alpha(D_d\theta)$ and the straight line $(D_s/D_{ds})(\theta-\theta_Q)$ (eq. [6] and Fig. 6*b*). The bottom sketch in Figure 6 is a schematic view of the images on the plane of the sky. Thus if the intercepts B1 and B2, at negative θ, are close together, the resulting (double) image is very bright, even though θ for that image is small. This situation may be the correct explanation for what is observed, although the presence of the cluster introduces some other possibilities. We will discuss these in § III*c*.

Let us first consider the modifications necessary to the treatment above when the object and the lens are at cosmological distances.

The geometry of gravitational lenses in a Robertson-Walker universe was treated by Gunn (1966). If the metric is written as

$$ds^2=c^2d\tau^2-R^2(\tau)\left[du^2+S_k^2(u)d\gamma^2\right], \quad (10)$$

where $S_k(u)=\sin u$, u, or $\sinh u$, depending on the topology, we may write

$$D_d=R_0S_k(u_d)(1+z_d)^{-1},$$

$$D_{ds}=R_0S_k(u_s-u_d)(1+z_s)^{-1},$$

$$D_s=R_0S_k(u_s)(1+z_s)^{-1}. \quad (11)$$

These expressions replace the Euclidean distances in Figure 6 and equations (4)–(9).

The D's can be written in closed form for any value of $\Omega=2q_0$ for a model with $\Lambda=0$ and no pressure. For our purposes the cases $\Omega=0$ and $\Omega=1$ suffice to illustrate the range of possibilities:

$$\Omega=0:S_k(u)=\tfrac{1}{2}\left[(1+z)-(1+z)^{-1}\right],$$

$$S_k(u_s-u_d)=\tfrac{1}{2}\left[(1+z_s)/(1+z_d)\right.$$

$$\left.-(1+z_d)/(1+z_s)\right]; \quad (12)$$

$$\Omega=1:S_k(u)=u=2\left[1-(1+z)^{-1/2}\right].$$

In both bases we can take $R_0=c/H_0$ (=5000 Mpc for $H_0=60$ km s^{-1} Mpc^{-1}). For the double quasar, $z_d=0.39$, $z_s=1.41$, and

$$D_d=(c/H_0)\times\{0.2412\quad(\Omega=0),0.2184\quad(\Omega=1)\},$$

$$D_{ds}=(c/H_0)\times\{0.2401\quad(\Omega=0),0.1693\quad(\Omega=1)\},$$

$$D_s=(c/H_0)\times\{0.4139\quad(\Omega=0),0.2954\quad(\Omega=1)\}. \quad (13)$$

In principle, the value of q_0 can be found from a measurement of the ratio of α to θ, which is derivable from observations of the velocity dispersion in the lens galaxy. But $\alpha/(\theta-\theta_Q)=D_s/D_{ds}$ which has the values 1.724 ($\Omega=0$) and 1.745 ($\Omega=1$). Thus in practice no cosmological information is likely to be obtained from the imaging geometry. The differential time delays from the various images are of the order of months, and are directly proportional to H_0^{-1} (Sanitt 1971). As we shall see in § III*c*, however, it will be difficult if not impossible to measure H_0 by this means because of the effects of the cluster.

b) Imaging by a King Model Galaxy

We shall apply the concepts sketched above to a spherically symmetric King (1966) model for the imaging galaxy. In dimensionless units the distribution function for the stars is

$$f(\varepsilon)=[\exp(-\varepsilon)-\exp(-\varepsilon_T)](2\pi)^{-3/2}, \quad (14)$$

where ε = dimensionless energy; ε_T = "cutoff" energy. The density is

$$\rho(\psi)=\exp(-\psi)\left[\mathrm{erf}(x)-2\pi^{-1/2}xe^{-x^2}(1+2x^2/3)\right], \quad (15)$$

where ψ is the dimensionless gravitational potential and $x^2=\varepsilon_T-\psi$. The scalar bend angle on passing through the King model is

$$\alpha_*=4\int_\beta^\infty \beta ds(s^2-\beta^2)^{-1/2}(d\psi/ds), \quad (16)$$

where s is the dimensionless radial coordinate (the unit of length is the structural length $a=\sigma_v(4\pi G\rho_0)^{-1/2}$, not the core radius $r_c=3a$), β is the dimensionless impact parameter, and α_* is the dimensionless bend angle in units of σ_v^2/c^2 (σ_v is the one-coordinate central velocity dispersion). The results of numerical integrations are shown in Figure 7 for $\varepsilon_T=10$, 12, and 14. The normal galaxy has a light distribution given by $\varepsilon_T=9$–10; but since mass-to-light ratios increase going outward in the one carefully studied cD galaxy (Dressler 1979), we shall use $\varepsilon_T=12$ for a representative galaxy model. Figure 7 shows that in the region of interest here ($\beta<30$) the models do not depend significantly on the value of ε_T.

A crucial property of the King models is that outside the core of the galaxy the bend angle $\alpha\approx 13(\sigma_v^2/c^2)$ is a slow function of the impact parameter β. This is because the density is $\rho\sim 2s^{-2}$, so the projected mass $\mathfrak{M}$ is proportional to β and the bend angle $4\,\mathfrak{M}/\beta$ is

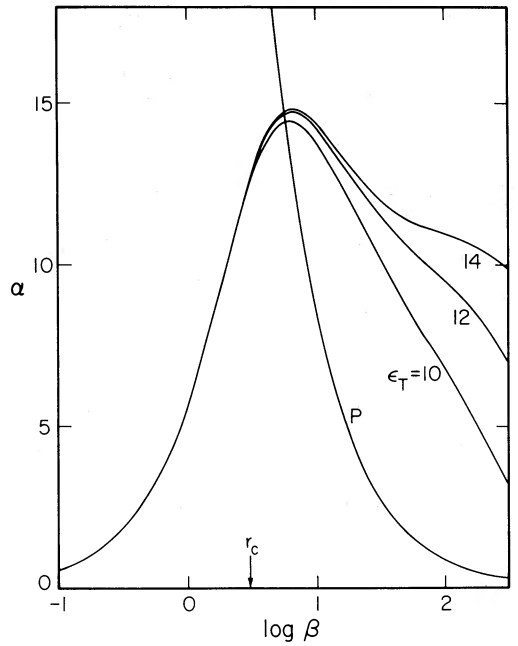

FIG. 7.—Gravitational bending angle α due to King model. α is in units of (σ_v^2/c^2) for an impact parameter β measured in units of the structural length $a=\sigma_v(4\pi G\rho_0)^{-1/2}$. The core radius r_c is at $\beta=3$. Models with dimensionless cutoff energy $\epsilon_T=10$, 12, and 14 are shown. Also shown is the β^{-1} power law for a point mass (P) to emphasize the different imaging properties of galaxies and point masses.

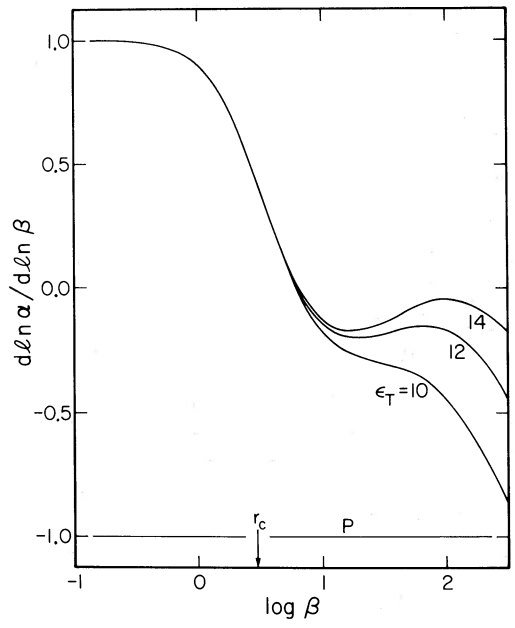

FIG. 8.—Dispersion of light rays passing near King model. Notation is the same as in Fig. 7.

nearly constant; for the limiting case of an isothermal sphere ($\epsilon_T=\infty$), $\alpha\to 4\pi(\sigma_v^2/c^2)$ as $\beta\to\infty$. The behavior is thus very different from that exhibited by a point mass acting as a lens.

To investigate the brightness amplification of the King models, it is necessary to know $(d\alpha_*/d\beta)$. It is more convenient to plot the quantity $d\ln\alpha_*/d\ln\beta$, which is shown in Figure 8 for the models of interest.

Useful interpolation formulae, which are accurate to $\sim$1% for $\beta<30$ in the case $\epsilon_T=12$, are as follows:

$$\alpha_*=53.2468\,f(0.385\beta)-44.0415\,f(0.193\beta), \tag{17}$$

$$d\alpha_*/d\beta=20.50\,h(0.385\beta)-8.50h(0.193\beta),$$

$$f(x)=\left[(1+x^2)^{1/2}-1\right]/x,$$

$$h(x)=\left[1-(1+x^2)^{-1/2}\right]/x^2.$$

It is now convenient to reduce the lens equations to dimensionless form. Let

$$q_1=(D_{ds}D_d/D_s a)(\sigma_v^2/c^2), \tag{18}$$

$$q_2=D_d/a.$$

Equation (6) becomes

$$\alpha_*(\theta^*)=(\theta^*-\theta_Q^*)/q_1, \tag{19}$$

with $\theta^*=q_2\theta$. Equation (9) becomes

$$I/I_0=(\theta^*/\theta_Q^*)\left[1-q_1\alpha_*'(\theta^*)\right]^{-1}. \tag{20}$$

Let images A, B1, and B2 be represented by appropriate suffixes. We must solve the following equations for q_1 and θ_Q^*:

$$\{|I_{B1}|+|I_{B2}|\}/|I_A|=0.75, \tag{21a}$$

$$\{|I_{B1}\theta_{B1}^*|+|I_{B2}\theta_{B2}^*|\}/|\theta_A^*|\{|I_{B1}|+|I_{B2}|\}=0.142, \tag{21b}$$

to give the observed brightness ratio of A to B1 plus B2, and also the observed ratio of distances from the galaxy.

We find the following solution for the $\varepsilon_T = 12$ King model:

$$\theta_Q^* = 15.0, \tag{22a}$$

$$q_1 = 1.3759, \tag{22b}$$

$$\theta_A^* = 30.865,\ I_A/I_0 = 1.880, \tag{22c}$$

$$\theta_{B1}^* = -3.824,\ I_{B1}/I_0 = 0.561, \tag{22d}$$

$$\theta_{B2}^* = -4.772,\ I_{B2}/I_0 = -0.846. \tag{22e}$$

With the observed angular separation of 6.″15 we also find

$$q_2 = 1.181 \times 10^6. \tag{22f}$$

The angular separation of images B1 and B2 is

$$|\theta_{B2} - \theta_{B1}| = 0.''16, \tag{23a}$$

with a brightness ratio

$$|I_{B2}/I_{B2}| = 1.51. \tag{23b}$$

Since the amplification is small (eqs. [22c–e]), the image sizes are not very different from the original source, and therefore too small for the image shapes to be of interest at present. We will discuss image shapes in a later paper. This solution gives

$$a = 1.02 \text{ kpc},\ \sigma_v = 425 \text{ km s}^{-1} \tag{24}$$

(using $q_0 = 0$). This core radius ($r_c = 3a = 3.06$ kpc) agrees well with the values in Hoessel (1980) for brightest cluster galaxies.

The elongation of B due to B1 and B2 components may be represented by its Gaussian standard deviation,

$$\sigma_B^2 = \sigma^2 + f(1-f)|\theta_{B2} - \theta_{B1}|^2, \tag{25}$$

where $f = |I_{B1}|/\{|I_{B1}| + |I_{B2}|\}$ and σ = seeing spread standard deviation. This would give $\theta_B = 0.''456$ if $\sigma = 0.''450$ and is not detectable in our CCD data. The splitting is quite sensitive to the uncertain effects of the cluster, which may give rise to images which are qualitatively different from the ones which we have just discussed.

c) Imaging by the Cluster

The cluster of galaxies surrounding the twin QSOs also acts as a lens and may not be neglected when considering the imaging by the galaxy. If the cluster has dimensions of ~200 kpc, it bends the light ray by ~10″ β_c inside its core (β_c = impact parameter/structural length) and by ~30″ outside the core. Since the QSO images are ~6″ apart and the cluster structural length is ~12″, it is clear that differential deflection by the cluster is important.

The cluster is likely to be too weak a lens to make three QSO images rather than one. However, the rays of light which pass near the galaxy are already being converged by the cluster lens and require only modest additional help from the galaxy to form multiple images.

The cluster is clearly *not* circularly symmetric on the sky, but the uncertainties in the cluster parameters are larger than the small effects of asymmetry in the projected mass distribution; we shall therefore make use of spherical cluster models, but with the cluster center not necessarily coincident with the galaxy center. Rather than attempt a complete solution of the image problem with many unknown parameters, we have tried to investigate the nature and degree of possible influence of the cluster on the final images by examining the solutions for various ranges of the parameters.

We shall now deal with a vector position on the sky $\boldsymbol{\theta}$, and a vector bending angle $\boldsymbol{\alpha}(\boldsymbol{\theta})$. If the true QSO position on the sky is $\boldsymbol{\theta}_Q$, we find

$$\boldsymbol{\theta} = \boldsymbol{\theta}_Q + (D_{ds}/D_d)\left[\boldsymbol{\alpha}_g(\boldsymbol{\theta}) + \boldsymbol{\alpha}_c(\boldsymbol{\theta})\right], \tag{26}$$

where $\boldsymbol{\alpha}_g$ and $\boldsymbol{\alpha}_c$ are the vector bending angles due to galaxy and cluster, respectively. We may reduce this to dimensionless form as before, giving

$$\boldsymbol{\theta}^* = \boldsymbol{\theta}_Q^* + q_1\left\{\boldsymbol{\alpha}_*(\boldsymbol{\theta}_g^*) + C\boldsymbol{\alpha}_*[\boldsymbol{\theta}_c^*(a/a_c)]\right\}, \tag{27}$$

where a_c is the structural length of cluster and $C = \sigma_v^2$ (cluster)/σ_v^2(galaxy). Then

$$\boldsymbol{\alpha}_*(\boldsymbol{\theta}^*) = \alpha_*(\theta^*)(\boldsymbol{\theta}^*/\theta^*), \tag{28}$$

where α_* is the dimensionless bending angle as previously defined, and $\boldsymbol{\theta}_g^*$ and $\boldsymbol{\theta}_c^*$ are, respectively, the image location with respect to the galaxy center and the cluster center, both in units of (a/D_d). We are thus using the King model with $\varepsilon_T = 12$ to represent both the galaxy and the cluster, but with different length and velocity scales. The image intensities are given by equation (7).

A Newton-Raphson procedure was used to solve for $\boldsymbol{\theta}^*$ in equation (27). By examining the solutions for

various values of the parameters, we found the imaging to be very complex and sensitive to the parameters chosen. The most critical parameter by far is the value of C in equation (27), which determines the relative strengths of the galaxy and cluster lenses. The following general features emerged:

The image separation is roughly doubled by a cluster-galaxy combination with $C=6$. In this case, the velocity dispersion of the galaxy is 360 km s^{-1}, and that of the cluster is 725 km s^{-1}.

Note that if the cluster dispersion is as high as 1100–1200 km s^{-1} (with a core radius $r_c=200$ kpc), then the cluster can, unaided, focus light upon the Earth. For even higher cluster velocity dispersions the cluster "overfocuses" like the galaxy and can itself produce further multiplicities of QSO images, highly amplified and at large distances from the cluster center.

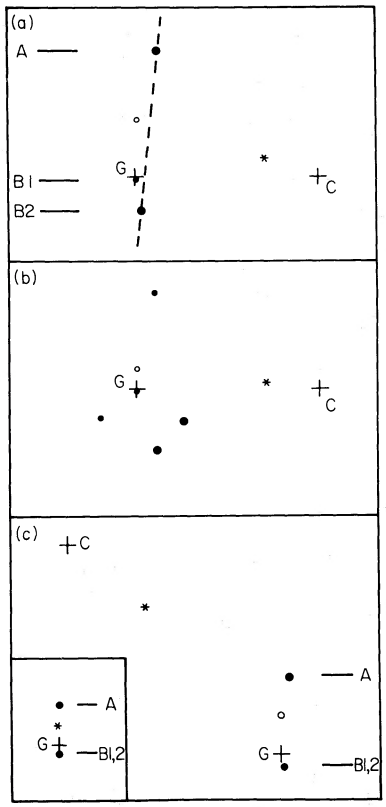

FIG. 9.—Some examples of imaging by a galaxy-cluster combination. In each diagram the cluster and galaxy centers are marked by pluses labeled C and G, respectively. The true QSO position is marked with an asterisk. The QSO as imaged by the cluster alone (ignoring the galaxy) is marked with an open circle. The actual images are marked with filled circles which are larger for brighter images. (*a*) An asymmetric distance ratio but with equal image brightnesses for A and B2. B1 is very faint. This also illustrates a strong "dogleg" in the image line and could describe Q0957+561 if our measured galaxy position is too far south. (*b*) A quintuple imaging solution. The extra images are the bright pair below and to the right of the galaxy. If the QSO is moved up, these images (which are of opposite parity) approach one another, become brighter, and then disappear. (*c*) Solution for a "double B" image. In this case images B1 and B2 are very close together (0.″15) and are in the brightness ratio 1.5 : 1. Note aso the "dogleg" in the image line, which is observed in Q0957+561 A, B. The inset shows the imaging obtained from the galaxy alone.

When the image line is perpendicular to the line from the galaxy center to the cluster center, differential cluster deflection can introduce a significant "dogleg" kink into what would otherwise be a straight galaxy–QSO image line. We show a typical dogleg situation in Figure 9*a*. This is a solution for the images with $C=7$, $q_1=1.5$, and $a/a_c=0.02$. In this case the image split increased by a factor of 2.9 when the cluster was included. This would correspond to galaxy and cluster velocity dispersions of 250 and 650 km s^{-1}, respectively.

Figure 9*a* illustrates another unexpected situation. The images A and B2 in this solution are of equal brightness despite being very unequal distances from the galaxy. Although it is hard to find solutions of this kind for angular distance ratios as large as 7 : 1 for A : B2, if our estimate of the position of the galaxy is in error we could easily have this type of solution. Solutions with equal brightness are easily found for distance ratios of 4 or 5. Thus the prediction that B may be double is uncertain. The third image (B1) in this case is 6.2 mag fainter than the primary image and would be very difficult to observe. The bright images are 5 and 4 times brighter than the true QSO, for images A and B2, respectively.

When the QSO image as produced by the cluster alone is close to the galaxy, higher order multiplicities can occur. This is illustrated in Figure 9*b*, which is a solution with $C=7$, $q_1=1.5$, and $a/a_c=0.02$. Although not applicable to Q0957+561, it illustrates the complexities of the galaxy-cluster combination.

Figure 9*c* shows a "double-B" solution similar to that sketched in Figure 6. Because of the complexity of the possible effects and the large number of ill-determined parameters, it is not possible to find a unique solution for the double QSO. Instead, we have sought a physically plausible solution involving the cluster and galaxy which reproduces our data. One such solution has:

$$\begin{aligned}
\text{Galaxy:}\quad & \sigma_v=320\text{ km s}^{-1},\\
& a=0.''171=1\text{ kpc},\\
& x=0,\\
& y=0;\\
\text{Cluster:}\quad & \sigma_v=1000\text{ km s}^{-1},\\
& a_c=-12.''0=70\text{ kpc},\\
& x=-15'',\\
& y=+15''. \qquad (29)
\end{aligned}$$

This reproduces the observed dogleg, image brightness, distance ratio, and image separation all as observed.

The cluster center and core radius are within observational errors. The cluster velocity dispersion is a guess. This solution does not uniquely define the parameters, but shows that the observed imaging can be modeled with reasonable values for them. One final comment is that the image doubling of B in this model was affected only very slightly by the addition of the cluster (which mainly moves image A away from the galaxy); the separation of B1 and B2 is 0.″15 and their brightness ratio is 1.45 (with the northern image fainter). The structural length of the galaxy in this model is given by the distance of B from the galaxy and is not sensitive to cluster effects. The amplification factor for image A is 7.5, or 2.2 mag.

The absolute visual magnitude of the QSO in this model is -25.8 (for $H_0=60$, $q_0=0$), which is still in the range of bright QSO luminosities. The Barnothys (see, for example, Barnothy and Barnothy 1968) have long been advocates of the formation of QSOs by the imaging of Seyfert nuclei by galaxies, but this object is intrinsically much too bright to be a Seyfert nucleus.

We have not attempted to calculate *a posteriori* a probability for this event; but for those who would do so, it is important to note that the lens almost certainly strongly amplifies both images, so the relevant surface density is that of quasars of about nineteenth, not seventeenth, magnitude.

The cluster has an additional unfortunate effect. The time delays among the various image paths are no longer predictable, unless the true QSO position on the sky is known. The differential time delay between two paths with total deflection angles α_1 and α_2 is proportional to $\alpha_2^2-\alpha_1^2\sim 2\alpha\Delta\alpha$ due to geometrical effects alone, and it is clear that the main effect of the cluster is to increase all time delays by a factor which can be as large as 25 and to scramble the differential delays.

d) *The Radio Structure*

Radio maps of Q0957+561 A, B have been presented by Pooley *et al.* (1979) and Roberts, Greenfield, and Burke (1979). With the insight gained from our investigation of the image problem, we feel that interpretation of the radio data will be very difficult. Certainly, simple arguments based on point-mass gravitational lenses are not likely to be applicable. Complication in the radio imaging include: (i) Extended features can be imaged in very complicated ways. (ii) The imaging galaxy may itself be a radio source.

If B is a double, nearly degenerate image, then the QSO lies just inside the singular circle around the galaxy where a source must lie to be triply imaged. The radio lobes named C, D, and E in Roberts, Greenfield, and Burke (1979) would then lie outside this circle and would be imaged singly. VLBI techniques would be best for detecting the double nature of B, if the QSO has a strong point source component.

A new VLA map (Greenfield, Roberts, and Burke 1980) shows a jet at p.a. 40° from Q0957+561 A, and another jet at p.a. 0° from Q0957+561 B. The jet in component A, in the model described by equation (29), would be intrinsic to the QSO and would be imaged until it hit the singular circle between the components of Q0957+561 B. The jet from Q0957+561 B passes through the center of the galaxy, and it is not clear where it originates. In our "double B" models it would have to come from the galaxy rather than from a QSO image. It is not unlikely that the galaxy, being the brightest galaxy in a rich cluster, is itself a radio source.

In the "single B" models with image dogleg produced by the cluster, the images can be both sheared and rotated (B would maintain an opposite parity to A, however). The exact nature of the distortions is critically dependent on the mass distribution in the cluster, which we shall investigate in a later paper. Lobes C, D, and E are likely to be too far away from the galaxy to be multiply imaged, but some structure may be not merely triply but quintuply imaged. It is, in particular, not only possible but easy to have jets at p.a. 40° and 0° in the A and B images. Any component of the B image jet which crosses the galaxy nucleus, however, cannot be imaged and once again we would have to invoke the galaxy itself as a possible radio source.

Porcas *et al.* (1979), in a discussion of their VLBI observations, say that the B image is unresolved ($\leq$ 0.″02) as is image A. We feel that this does not yet rule out a "double B" solution for the following reasons:

i) Depending on the mass distribution of the galaxy core, the brightness ratio of B1 to B2 can be different from 1.5:1.

ii) If the galaxy is actually somewhat farther away from the B image than our estimate of 0.″78, then the images separate and B2 can once again be quite faint.

iii) If the ratio is larger than 1.5, data with higher dynamic range may be required for the duplicity to be detected.

IV. SUMMARY

Deep CCD pictures show a rich cluster of galaxies around the double quasar Q0957+561, as well as faint extended wings on the image of the southern QSO (B). This extended image, which is faint, elliptical, and off-center from the QSO image, has the appearance of a galaxy seen in projection against the QSO. We believe that it is the brightest cluster galaxy, and that it and the cluster in combination act as a gravitational lens to image a single distant QSO into the double image seen.

The argument is based on the following considerations:

1. The spectrum of QSO component B shows a strong break, not present in the spectrum of A, at λ5500, as well as a greater relative flux at longer wavelengths. If this difference is assumed to be due to

the extended image around B, interpreted as a foreground galaxy, it has a redshift of $0.39 \pm .02$.

2. The size and brightness of the cluster are consistent with this redshift.

3. The extended image around B has the size, brightness, and appearance of a bright cluster galaxy at this redshift. In particular, it appears very similar to the galaxy G2, which is nearly as bright but lies well away from the QSO images. If the redshift of G2 or other galaxies in the cluster is found to be near 0.39, it will eliminate any remaining doubt of our interpretation of the data.

4. Models of the gravitational imaging, assuming that G1 is a King model galaxy at $z = 0.39$, give a core radius for the galaxy consistent with those of other bright cluster galaxies.

5. The models, including the effect of the cluster, are able to reproduce the observed data, although they do not do so uniquely because of the present lack of data.

We conclude that the double quasar Q0957+561 A, B is almost certainly two images of a single object formed by a gravitational lens. The details of the imaging are unclear because of the uncertainties in the physical parameters, the most important of which are the velocity dispersions in the galaxy and cluster, and the location of the effective cluster center. With quite plausible values for these parameters, images like those observed are produced, and in fact one has at least two choices for the qualitative features of the model.

A possible consequence is that the B image is double with a roughly north-south separation of $\sim 0\farcs16$ with an intensity ratio of $\sim 1.6 : 1$. This separation should be looked for by high-resolution optical or radio techniques. The structure of the B image, if double, is very sensitive to the distribution of mass in the core region of the imaging galaxy. When high-resolution optical images are available from the Space Telescope, a comparison can be made between the distribution of mass and of light in a giant elliptical galaxy.

Even with good measurements of presently uncertain parameters, it seems doubtful that any of the elegant cosmological tests proposed by several authors in the past can be applied with sufficient accuracy to be useful.

A more accurate model can, however, provide a crude test of general relativity over scales ($\sim$200 kpc) much larger than those accessible by any other means. If velocity dispersions in the cluster *and* the galaxy can be measured, one can test whether the coefficient in equation (2) is in fact equal to 2 on large scales.

It is, perhaps, unfortunate that the first case of gravitational imaging is so complex, but it seems in hindsight not unlikely. Massive galaxies are more often than not found in clusters and groups. Searches for other cases, some of which might be simple, should be encouraged. Especially promising are high-redshift QSOs with moderate redshift ($z \sim 0.4$–0.6) absorption systems, a review of which was given a few years ago by Sanitt (1971).

We wish to thank Dr. Bernard Burke and Dr. Alan Stockton for data in advance of publication, Juan Carrasco for expert assistance at the telescope, and James Janesick, Ernest Lorenz, Richard Lucinio, Victor Nenow, and Devere Smith for technical assistance with the CCD instrument. This research was supported in part by the National Science Foundation, grants AST76-80801, 77-04182, and 78-24842, and by the National Aeronautics and Space Administration through contract NGL 05-002-134.

REFERENCES

Adams, M. T., and Boroson, T. A. 1979, *Nature*, **282**, 183.
Barnothy, J. M., and Barnothy, M. F. 1968, *Science*, **162**, 348.
Bourassa, R. R., and Kantowski, R. 1975, *Ap. J.*, **195**, 13.
Dressler, A. 1979, *Ap. J.*, **231**, 659.
Greenfield, P. E., Roberts, D. H., and Burke, B. F. 1980, *Science*, **208**, 495.
Gunn, J. E. 1966, *Ap. J.*, **147**, 61.
Gunn, J. E., Hoessel, J., and Westphal, J. 1980, in preparation.
Hoessel, J. 1980, *Ap. J.*, in press.
Hoessel, J., Gunn, J. E., and Thuan, T. X. 1980, *Ap. J*, in press.
King, I. R. 1966, *A.J.*, **71**, 64.
Oke, J. B. 1969, *Pub. A.S.P.*, **81**, 11.
Pooley, G. G., Browne, I. W. A., Daintree, E. J., Moore, P. K., Noble, R. G., Walsh, D. 1979, *Nature*, **280**, 461.
Porcas, R. W., Booth, R. S., Browne, I. W. A., Walsh, D., and Wilkinson, P. N. 1979, *Nature*, **282**, 385.
Roberts, D. H., Greenfield, P. E., Burke, B. F. 1979, *Science*, **205**, 894.
Sanitt, N. 1971, *Nature*, **234**, 199.
Sebok, W. L. 1979, *A.J.*, **84**, 1526.
Thuan, T. X., and Gunn, J. E. 1976, *Pub. A.S.P.*, **88**, 543.
Walsh, D. Carswell, R. F., and Weymann, R. J. 1979, *Nature*, **279**, 381.
Weymann, R. J., Chaffee, F. H., Davis, M., Carleton, N. P., Walsh, D., and Carswell, R. F. 1979, *Ap. J. (Letters)*, **233**, L43.
Wills, B. J. and Wills, D. 1980, *Ap. J.*, **238**, 1.
Young, P. J, Sargent, W. L. W., Kristian, J., and Westphal, J. A. 1979, *Ap. J.*, **234**, 76.

JAMES E. GUNN, J. B. OKE, and PETER YOUNG: Robinson Laboratory of Astrophysics, California Institute of Technology, 1201 East California Blvd., Pasadena, CA 91125

JEROME KRISTIAN: Mount Wilson and Las Campanas Observatories, 813 Santa Barbara St., Pasadena, CA 91101

JAMES A. WESTPHAL: Department of Geology and Planetary Science, California Institute of Technology, 1201 East California Blvd., Pasadena, CA 91125